Journal of Magnetic Resonance 308 (2019) 106562

Contents lists available at ScienceDirect

Journal of Magnetic Resonance

journal homepage: www.elsevier.com/locate/jmr

Nuclear magnetic resonance T_1–T_2 inversion with double objective functions

Jiangfeng Guo, Ranhong Xie *, Lizhi Xiao, Guowen Jin, Lun Gao

State Key Laboratory of Petroleum Resources and Prospecting, China University of Petroleum (Beijing), Beijing 102249, China
Key Laboratory of Earth Prospecting and Information Technology, China University of Petroleum (Beijing), Beijing 102249, China

ARTICLE INFO

Article history:
Received 17 June 2019
Revised 15 July 2019
Accepted 16 July 2019
Available online 17 July 2019

Keywords:
Nuclear magnetic resonance (NMR)
T_1–T_2
Inversion
L1 regularization
Least-squares principle

ABSTRACT

We report an effective and robust method for nuclear magnetic resonance (NMR) longitudinal relaxation time–transverse relaxation time (T_1–T_2) inversion with double objective functions. First, we develop the first objective function based on L1 regularization, proposed an effective method to choose the optimum L1 regularization parameter, and solve the objective function employing a two-step iterative shrinkage/thresholding algorithm. Subsequently, we update the kernel matrix based on the solution of the first objective function, and then develop the second objective function using the measured data and updated kernel matrix based on the least-squares principle, and we use the conjugate gradient algorithm for the first time to solve the objective function about NMR data inversion. To improve the speed of NMR T_1–T_2 inversion, we present a Gaussian-based random SVD method. Finally, numerical and experimental examples are done to test the robustness of the proposed inversion method. The results indicate that the proposed inversion method can effectively achieve NMR T_1–T_2 inversion at a low data SNR.

1. Introduction

Nuclear magnetic resonance (NMR) is a sophisticated technology today, and it has been broadly applied in the areas of physics, chemistry, medicine and geoscience [1–5]. For example, NMR technology in geoscience is commonly used to identify fluid types and calculate reservoir petrophysical parameters like porosity, pore structure, wettability, permeability and bound water saturation [4–10]. Measured relaxation information about longitudinal relaxation time (T_1) or transverse relaxation time (T_2) by NMR is tightly associated with the sample physical and structural properties, so NMR measurement is a powerful tool to characterize the sample components and structures. Unfortunately, the signals of different components for a complex sample sometimes overlap in one-dimensional (1D) NMR map, leading to the misunderstandings of the sample components. Two-dimensional (2D) NMR can provide more detailed and more information than 1D NMR [11–13], and T_1–T_2 measurement that can acquire T_1 and T_2 information simultaneously is an example. Hence, interpreting the properties of the mixture is more accurate based on the T_1–T_2 map than based on the single T_1 or T_2 map.

However, measured 2D NMR signals do not directly exhibit different relaxation components. It is wise to invert the signals into intuitive 2D NMR map, but the inversion problem is an ill-posed, which means that little changes in the collected signals can make huge differences in the inverted NMR map, especially when signal-to-noise ratio (SNR) of signal is low. Researchers have given much time and attention to focus on developing accurate 2D NMR map inversion methods. We categorize the inversion methods into explicit regularization methods and iterative methods according to the form of the objective function. The objective functions of explicit regularization methods consist of a regularization term and a fitting residual term. Different regularization methods have different penalty functions in the regularization term. Venkataramanan et al. [12], Song et al. [13] used Frobenius norm of the solution as the penalty function, known as L2 regularization. The Butler–Reeds–Dawson (BRD) algorithm [14] and Levenberg–Marquardt (LM) algorithm [15] can be used for solving the L2 regularization. Provencher [16] used the second derivative operator of the solution as the penalty function, which can be solved by the CONTIN algorithm. Unfortunately, the inverted NMR maps by this algorithm are characterized by over-smoothed weak peaks and under-smoothed strong peaks. Chouzenoux et al. [17] used the standard Shannon entropy of the solution as the penalty function, known as maximum entropy regularization, and then Zou et al. [18] developed a modified Shannon entropy function as the penalty function, and

* Corresponding author.
E-mail address: xieranhong@cup.edu.cn (R. Xie).

https://doi.org/10.1016/j.jmr.2019.07.049
1090-7807/

applied the LM algorithm for solving the objective function. Zhou et al. [19], Reci et al. [20], and Guo et al. [21] utilized the L1 norm of the solution as the penalty term, known as L1 regularization, which can be solved by the iterative shrinkage/thresholding (IST) algorithm or the primal-dual hybrid gradient algorithm. The sparse NMR map can then be obtained using the L1 regularization method, but selecting the optimum L1 regularization parameter is the major obstacle. Unlike the above-stated regularization method with a regularization term, Berman et al. [22], Wang et al. [23], and Guo et al. [24] implemented two different penalty functions with different regularization parameters, unfortunately, there has not been unified standard for selecting the two regularization parameters.

The iterative method does not have a regularization term in the objective function. Prammer [6] first proposed the truncated singular value decomposition (TSVD) algorithm to invert NMR data. Subsequently, the TSVD algorithm was improved continually by some researchers [25–27]. Sadly, the inverted NMR maps by the TSVD algorithm are not ideal for a low SNR data. Sebastião and Braga [28] and Sebastião et al. [29] inverted NMR echo data using the Hopfield neural network method to retrieve T_2 map and diffusion coefficient map. The least-squares QR decomposition (LSQR) algorithm proposed by Paige and Saunders [30] is an algorithm of solving the least-squares problem with a Lanczos iteration. Tan et al. [11,31] first used the LSQR algorithm to invert NMR echo data, and proposed an LSQR–TSVD hybrid inversion algorithm, and concluded that the accuracy was higher for the hybrid algorithm than for the single algorithm. Su et al. [32] proposed an adaptive NMR inversion algorithm combining the LSQR and L curve. The inverted NMR maps by the LSQR algorithm usually exhibit some fake peaks, which sometimes lead to wrong estimate for the real components. Wang et al. [33] proposed a simultaneous iterative reconstruction technique (SIRT) algorithm. The initial values of the SIRT algorithm affect the precision and convergence rate; the inverted NMR map with a long relaxation time from the SIRT algorithm may show many peaks for a low SNR data.

The above descriptions show that the existing inversion methods have their respective shortcomings and need improvement. Traditional inversion methods are based on the idea of solving an objective function of NMR inversion problem with different algorithms, but sometimes it is not enough just to use an objective function during NMR map inversion. In this paper, a novel method for NMR map inversion based on double objective functions was proposed. The first objective function is established based on L1 regularization, and the second objective function is established based on the least-squares principle and the solution of the first objective function. In addition, the amount of the measured 2D T_1–T_2 data is very large, so the data inversion is time-consuming and requires a huge amount of memory. Considering the problem of 2D data quantity, an efficient method was proposed to compress NMR data. Finally, the robustness and effectiveness of the proposed method were tested by numerical and experimental examples.

2. Problem statement

NMR T_1–T_2 measurement can acquire T_1 and T_2 information simultaneously, which helps us to distinguish each component of measured samples. The inversion-recovery (IR) Carr–Purcell–Meiboom–Gill (CPMG) pulse sequence is usually used for T_1–T_2 measurement due to its high resolution for a short T_1 component. The measured echo data using the IR CPMG pulse sequence can be written based on the Fredholm integral equation of the first kind

$$Y(TW,t)=\iint\left[1-2\exp\left(-\frac{\mathrm{TW}}{T_1}\right)\right]\exp\left(-\frac{t}{T_2}\right)S(T_1,T_2)dT_1dT_2+\mathrm{E}(\mathrm{TW},t) \tag{1}$$

where t is the measuring time; $Y(\mathrm{TW},t)$ are the measured echo data at time t as wait time is TW; $S(T_1,T_2)$ is the unknown T_1–T_2 map to solve; and $\mathrm{E}(\mathrm{TW},t)$ is the noise.

The discrete form of Eq. (1) can be expressed as

$$Y(TW_m,t_i)=\sum_{j}^{J}\sum_{p}^{P}\left[1-2\exp\left(-\frac{\mathrm{TW}_m}{T_{1,p}}\right)\right]\exp\left(-\frac{t_i}{T_{2,j}}\right)S(T_{1,p},T_{2,j})+\mathrm{E}(\mathrm{TW}_m,t_i) \tag{2}$$

where $Y(\mathrm{TW}_m,t_i)$ and $\mathrm{E}(\mathrm{TW}_m,t_i)$ are the measured echo data and noise with the mth (m = 1, 2, 3, …, M) wait time at time t_i (i = 1, 2, 3, …, I); $S(T_{1,p},T_{2,j})$ is the $(T_{1,p},T_{2,j})$ amplitude in the unknown T_1–T_2 map to solve.

The matrix form of Eq. (2) is written as

$$\mathbf{Y}=\mathbf{K_1}\mathbf{S}\mathbf{K_2^{\mathrm{T}}}+\mathbf{E} \tag{3}$$

where $\mathbf{Y}$ and $\mathbf{E}$ with a size of $M\times I$ are the measured echo data and noise; the elements of $\mathbf{K}_1$ with a size of $M\times P$ are $K_1(m,p)=1-2\exp\left(-\frac{\mathrm{TW}_m}{T_{1,p}}\right)$; the elements of $\mathbf{K}_2$ with a size of $I\times J$ are $K_2(i,j)=\exp\left(-\frac{t_i}{T_{2,j}}\right)$; $\mathbf{S}$ with a size of $P\times J$ is the unknown T_1–T_2 map to solve; superscript T stands for the transpose of matrix.

The 2D NMR map inversion problem can be described as a problem of how to solve $\mathbf{S}$ under the condition that the measured data $\mathbf{Y}$ and the kernel matrices $\mathbf{K}_1$ and $\mathbf{K}_2$ are known. In a 2D NMR inversion problem, 2D problem is usually transformed to a 1D problem, which is then solved using an inversion algorithm; subsequently, the 1D solution is reallocated to a 2D space. Thus, it would be obtain

$$\mathbf{y}=\mathbf{K}\mathbf{s}+\mathbf{e} \tag{4}$$

where $\mathbf{y}=\mathrm{vect}(\mathbf{Y})$; $\mathbf{s}=\mathrm{vect}(\mathbf{S})$; $\mathbf{e}=\mathrm{vect}(\mathbf{E})$;$\mathbf{K}=\mathbf{K_1}\otimes\mathbf{K_2}$; vect() represents the operator establishing a new vector through stacking all the columns of a matrix; $\otimes$ represents the Kronecker product of two matrices.

NMR data inversion, solving $\mathbf{s}$ according to Eq. (4), is an ill-posed problem. More careful attention should be paid to the inversion to improve the precision of NMR data processing.

3. Methods

3.1. Compression method

Considering the large size of 2D NMR datasets, the measured data $\mathbf{y}$ and kernel matrix $\mathbf{K}$ in Eq. (4) were usually compressed before inversion to improve the inversion speed [34,35]. The SVD method is the most popular compression method, but it is time-consuming because of SVD of kernel matrix $\mathbf{K}$. In this paper, a Gaussian-based random SVD method was proposed to compress the NMR data; in this method, a low-dimensional matrix is developed based on kernel matrix $\mathbf{K}$ and subsequently an SVD is implemented for the low-dimensional matrix to obtain the compression matrix [36], so the proposed method can save a large amount of time in the SVD of matrix. First, a random matrix $\mathbf{Q}$ satisfying Eq. (5) was constructed based on random sampling,

$$\mathbf{K}\approx\mathbf{Q}\mathbf{Q}^{\mathrm{T}}\mathbf{K} \tag{5}$$

Then, a low-dimensional matrix $\mathbf{T}$ was given by

$$\mathbf{T}=\mathbf{Q}^{\mathrm{T}}\mathbf{K} \tag{6}$$

Finally, we complement SVD for matrix **T** rather than matrix **K**. Obviously, the former saves much time to perform SVD.

The detailed steps of the method are as follows: (1) input the kernel matrix **K**, measured data *y*, and compression number *nc*; (2) determine the column of **K** and develop a Gaussian-based random matrix **P** with a size of $n \times nc$; (3) calculate **W** = **KP** and obtain the orthonormal matrix **Q** of the matrix **W** using QR decomposition; (4) calculate the low-dimensional matrix $\mathbf{T} = \mathbf{Q}^{\mathrm{T}}\mathbf{K}$ and perform an SVD of the matrix $\mathbf{T} = \mathbf{U}\Sigma\mathbf{V}^{T}$; (5) calculate the new matrix $\widehat{\mathbf{U}} = \mathbf{QU}$ and output the kernel matrix $\widehat{\mathbf{K}} = \widehat{\mathbf{U}}^{\mathrm{T}}\mathbf{K}$ and measured data $\widehat{\mathbf{y}} = \widehat{\mathbf{U}}^{\mathrm{T}}\mathbf{y}$ after compression. Therefore, the flowchart of Gaussian-based random SVD method to compress NMR data was given in Fig. 1.

3.2. Inversion method

Proper objective function is essential for the inversion of T_1–T_2 map. An objective function is usually developed based on the measured data and constructed kernel matrix in the traditional inversion methods. The inversion results may deviate from the true solution for the noisy data, especially for low SNR data. In this study, a novel method to invert NMR map was proposed based on double objective functions. First, an objective function based on L1 regularization was developed, which can be written as [19,21]

$$\arg\min_{\mathbf{s}\geqslant 0} L(\mathbf{s}) = \frac{1}{2}\| \mathbf{y} - \mathbf{Ks} \|_2^2 + \lambda \| \mathbf{s} \|_1 \tag{7}$$

where $\lambda > 0$ is the L1 regularization parameter that controls the weight of the residual and the regularization term. Subsequently, the kernel matrix was updated based on the solution of Eq. (7). Then, another objective function was developed from the measured data and the updated kernel matrix based on least-squares principle, which can be written as

$$\arg\min_{\mathbf{s}^*\geqslant 0} L^*(\mathbf{s}) = \frac{1}{2}\| \mathbf{y} - \mathbf{K}^*\mathbf{s}^* \|_2^2 \tag{8}$$

where $\mathbf{K}^*$ is the sub-matrix of **K** obtained by deleting the columns of **K** corresponding the solution **s** of Eq. (7) equaling to 0. Finally, the solution $\mathbf{s}^*$ of Eq. (8) was solved, and the nonzero elements of **s** were sequentially replaced with the elements of $\mathbf{s}^*$ to obtain the final inversion solution. The aim of the second objective function [Eq. (8)] is to optimize the solution of the first objective function [Eq. (7)] and make the final solution closer to the true solution.

Eq. (7) can be solved by many algorithms, such as primal-dual hybrid gradient algorithm and IST algorithm. However, each iterative solution depends only on the previous iterative solution for these algorithms, so the convergence speeds of the algorithms need to be improved. Thus, Eq. (7) was solved using a two-step IST (TIST) algorithm [21,37] that each iterative solution depends on the two previous ones and the convergence speed is faster. The iterative approach can be expressed as

$$\mathbf{s}_2 = \Psi_\lambda\left(\mathbf{s}_1 + \mathbf{K}^T(\mathbf{y} - \mathbf{Ks}_1)\right) \tag{9}$$

$$\mathbf{s}_{t+1} = (1-\alpha)\mathbf{s}_{t-1} + (\alpha-\beta)\mathbf{s}_t + \beta\Psi_\lambda\left(\mathbf{s}_t + \mathbf{K}^T(\mathbf{y} - \mathbf{Ks}_t)\right), \quad t > 1 \tag{10}$$

where *t* is the iteration time; $\mathbf{s}_t$ is the *t*th iterative solution; α and β are step size parameters ($\alpha \neq 1$, $\beta \neq 1$); and Ψ_λ is the soft thresholding function, that is expressed as

$$\Psi_\lambda(x) = \mathrm{soft}(x,\lambda) = \mathrm{sign}(x)\max(|x| - \lambda, 0). \tag{11}$$

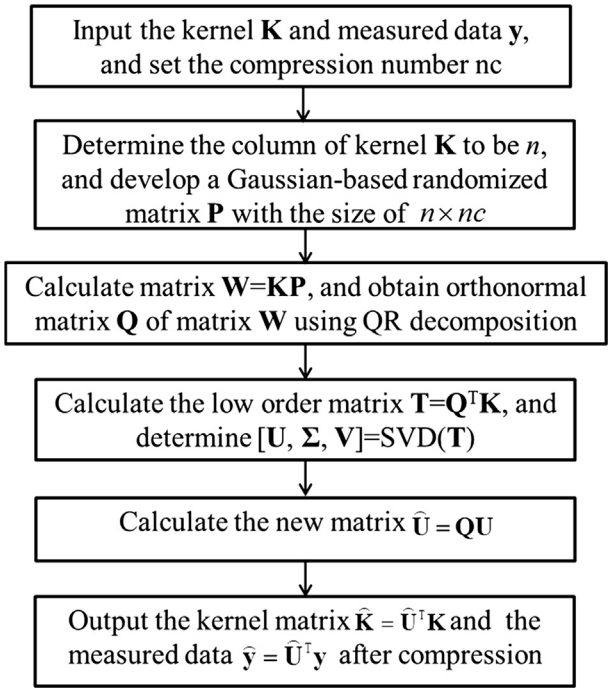

Fig. 1. Flowchart of the Gaussian-based random SVD method for NMR data compression.

To guarantee convergence of the algorithm, the objective function value $L(\mathbf{s})$ should be reduced after each iteration, i.e., $L(\mathbf{s}_{t+1}) \leqslant L(\mathbf{s}_t)$. However, $L(\mathbf{s}_{t+1})$ may be larger than $L(\mathbf{s}_t)$ using the iteration of Eq. (10). The algorithm at $\alpha = \beta = 1$ is convergent, and the proof is shown in [38]. Thus, we replace Eq. (10) with $\mathbf{s}_{t+1} = \Psi_\lambda\left(\mathbf{s}_t + \mathbf{K}^T(\mathbf{y} - \mathbf{Ks}_t)\right)$ when $L(\mathbf{s}_{t+1}) > L(\mathbf{s}_t)$. Comprehensively, we would implement the following iteration for $t > 1$,

$$\mathbf{s}_{t+1} = \begin{cases} \Psi_\lambda\left(\mathbf{s}_t + \mathbf{K}^T(\mathbf{y} - \mathbf{Ks}_t)\right), & L(\mathbf{m}) > L(\mathbf{s}_t) \\ \mathbf{m}, & L(\mathbf{m}) \leqslant L(\mathbf{s}_t) \end{cases} \tag{12}$$

where **m** is determined from Eq. (10); and $L(\mathbf{s}_t)$ is the value of objective function [Eq. (7)] at iteration time $t-1$.

Many optimization algorithms can be used for solving Eq. (8), including the steepest descent (SD) algorithm, the conjugate gradient (CG) algorithm and the Newton algorithm among others [39–41]. These algorithms have been widely used for the inversion of seismic data, magnetotelluric sounding data, and heat conduction. However, the CG algorithm overcomes the shortcoming of the SD algorithm that has a very slow convergence speed and avoids the shortcoming of the Newton algorithm that computes Hessian matrix and its inverse matrix, and it is a revision of the conjugate direction algorithm. Based on this, the CG algorithm was used to solve Eq. (8). If the solution of Eq. (7) is expressed as $\mathbf{s}_{old}$, the initial solution of Eq. (8) could be written as $\mathbf{s}_1^*$ that is the sub-matrix of $\mathbf{s}_{old}$ obtained by deleting all elements with a value of 0. In the CG algorithm, the initial search direction $\mathbf{d}_1 = \mathbf{y} - \mathbf{K}^*\mathbf{s}_1^*$ and the *k*th search direction $\mathbf{d}_{k+1}$ is a linear combination of the negative gradient $-\nabla L^*(\mathbf{s}_{k+1}^*)$ and the previous search direction $\mathbf{d}_k$, given by

$$\mathbf{d}_{k+1} = \mathbf{d}_k - \alpha_{k+1}^* \nabla L^*(\mathbf{s}_{k+1}^*) \tag{13}$$

where α_{k+1}^* is the combination coefficient at the *k*th iteration. For $k \geqslant 1$, the solution $\mathbf{s}_{k+1}^*$ for Eq. (8) can be calculated from $\mathbf{s}_k^*$ by means of a line search along $\mathbf{d}_{k+1}$. Therefore, the iteration scheme

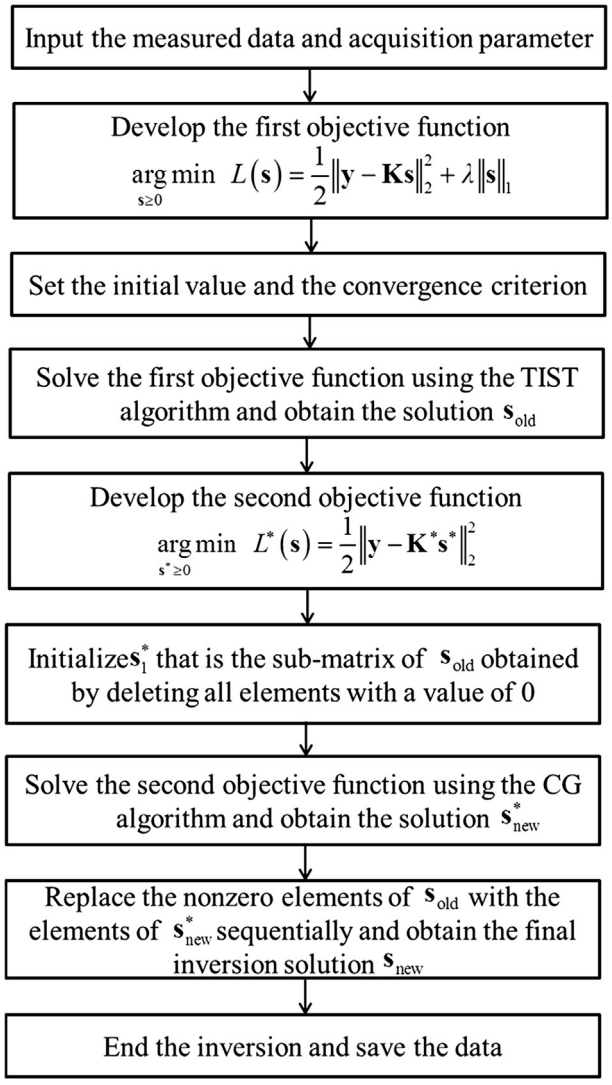

Fig. 2. Flowchart of the proposed inversion method.

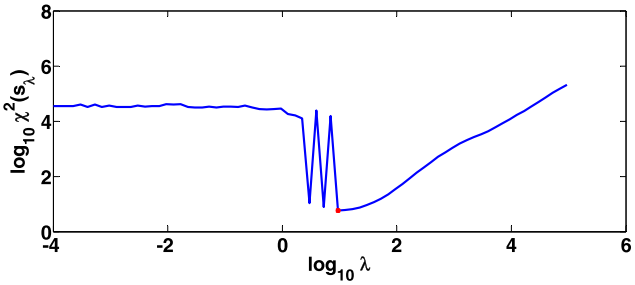

Fig. 3. Diagram of the logarithmic relationship between the residual $\chi^2(\mathbf{s}_\lambda)$ and the L1 regularization parameter λ.

of the CG algorithm for solving Eq. (8) can be expressed as Eqs. (14)–(20), and the iteration time k is more than 0.

$$\mathbf{q}_{k+1} = \mathbf{K}^*\mathbf{p}_{k+1} \tag{14}$$

$$\alpha_{k+1}^* = \| \boldsymbol{\theta}_k \|_2^2 / \| \mathbf{q}_{k+1} \|_2^2 \tag{15}$$

$$\mathbf{s}_{k+1}^* = \mathbf{s}_k^* + \alpha_{k+1}^*\mathbf{p}_{k+1} \tag{16}$$

$$\mathbf{d}_{k+1} = \mathbf{d}_k - \alpha_{k+1}^*\mathbf{q}_{k+1} \tag{17}$$

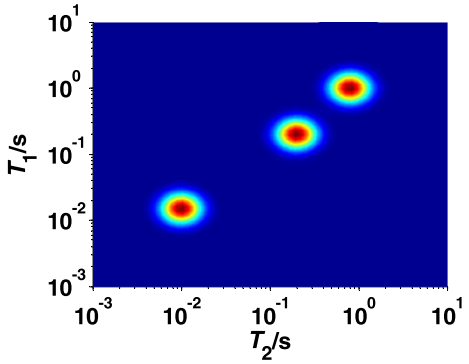

Fig. 4. Oil-water T_1–T_2 map model.

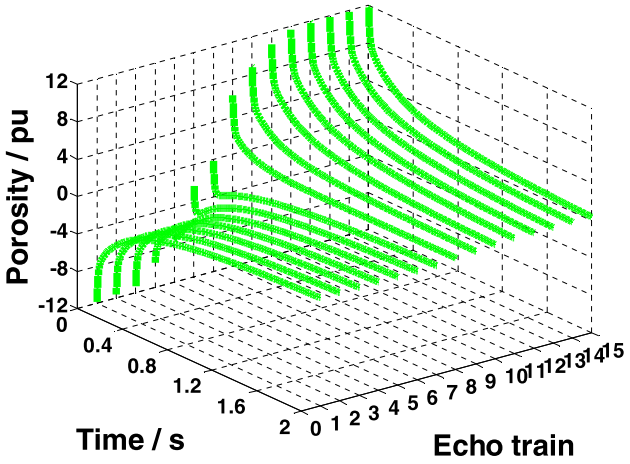

Fig. 5. Calculated echo data of oil-water model without noise.

$$\boldsymbol{\theta}_{k+1} = (\mathbf{K}^*)^{\mathrm{T}}\mathbf{d}_{k+1} \tag{18}$$

$$\beta_{k+1}^* = \| \boldsymbol{\theta}_{k+1} \|_2^2 / \| \boldsymbol{\theta}_k \|_2^2 \tag{19}$$

$$\mathbf{p}_{k+2} = \boldsymbol{\theta}_{k+1} + \boldsymbol{\beta}_{k+1}^*\mathbf{p}_{k+1} \tag{20}$$

where the initial value $\mathbf{p}_2 = \boldsymbol{\theta}_1 = (\mathbf{K}^*)^{\mathrm{T}}\mathbf{d}_1$.

The proposed inversion method was summarized in the flowchart, as shown in Fig. 2.

3.3. Choice of L1 regularization parameter λ

The regularization parameter provides a tradeoff between regularity and fidelity-to-data; the parameter directly determines the quality of the inversion results [12,17,42]. Hence, when the first objective function [Eq. (7)] is solved, choosing an appropriate L1 regularization parameter is of significance. In this study, an effective method for choosing L1 regularization parameter was proposed.

The residual with different regularization parameters can be calculated from

$$\chi^2(\mathbf{s}_\lambda) = \frac{1}{2}\| \mathbf{K}\mathbf{s}_\lambda - \mathbf{y} \|_2^2 \tag{21}$$

where $\mathbf{s}_\lambda$ is the solution of the first objective function with the regularization parameter λ.

The logarithmic relationship between the residual $\chi^2(\mathbf{s}_\lambda)$ and the L1 regularization parameter λ can be plotted, as shown in Fig. 3. Different from the L2 regularization method, the residual for the L1 regularization method does not increase with the

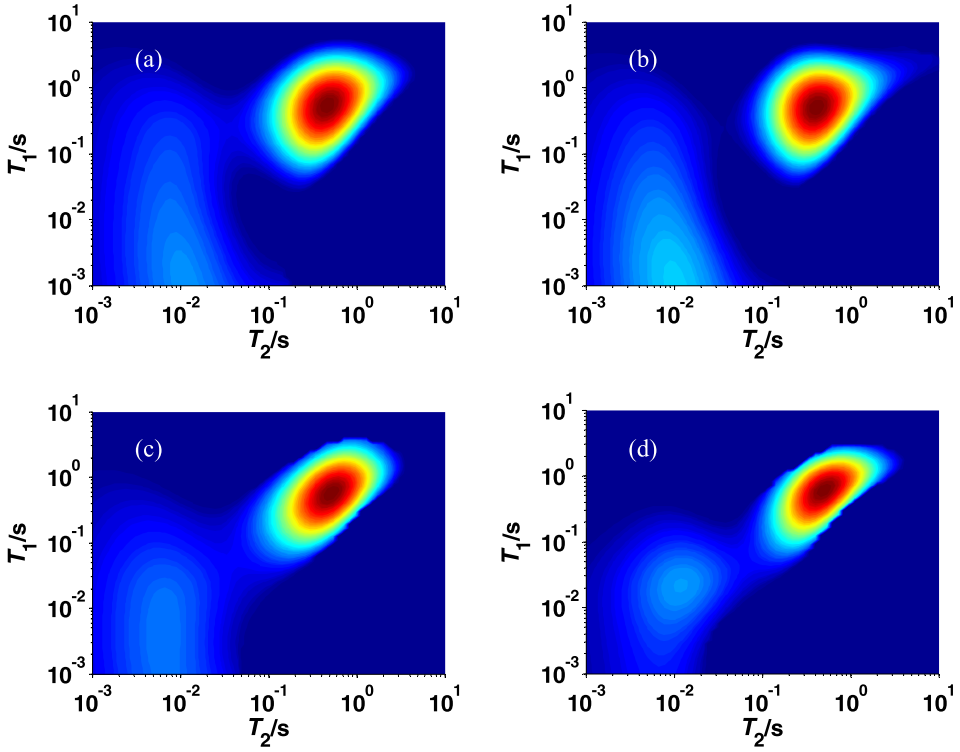

Fig. 6. Inverted T_1–T_2 maps of oil-water model with different SNRs using the TSVD method. (a) SNR = 5; (b) SNR = 10; (c) SNR = 20; (d) SNR = 40.

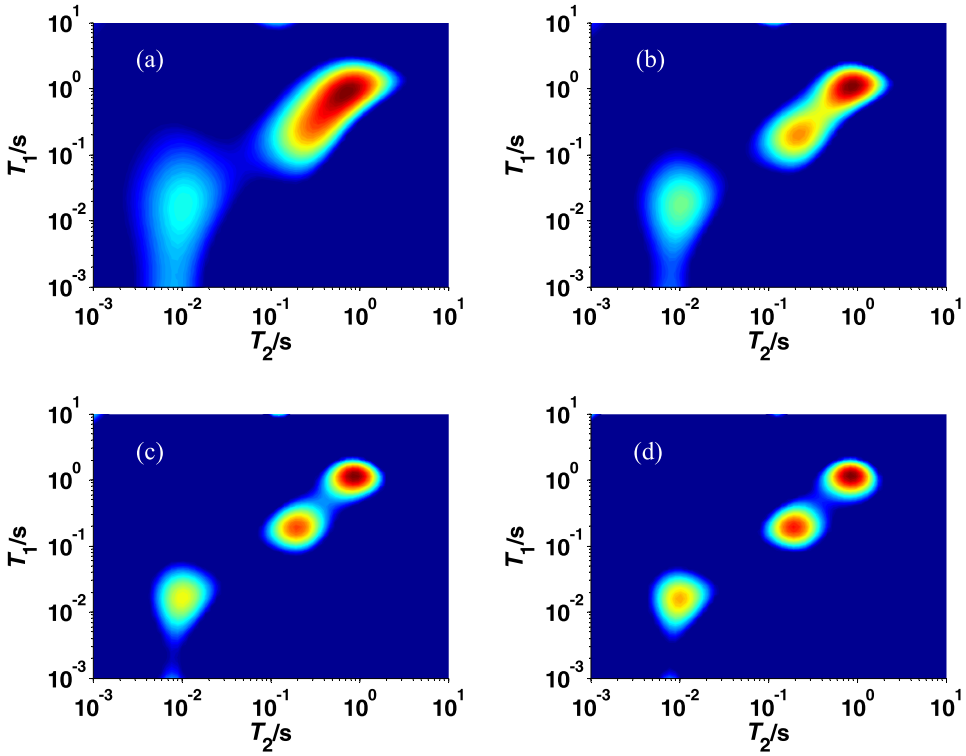

Fig. 7. Inverted T_1–T_2 maps of oil-water model with different SNRs using the norm smoothing method. (a) SNR = 5; (b) SNR = 10; (c) SNR = 20; (d) SNR = 40.

increase in the value of the regularization parameter. Fortunately, too large or too small L1 regularization parameter results in a high residual from Fig. 3. The global minimum residual can be found at the red[1] point in Fig. 3, and the corresponding $\mathbf{s}_\lambda$ is considered as the optimum solution of Eq. (7), thus the corresponding λ is the optimum L1 regularization parameter.

Above all, only calculate the residuals with different regularization parameters, and then obtain the optimum L1 regularization parameter λ_{opt} which is the corresponding λ with the smallest residual.

[1] For interpretation of color in Fig. 3, the reader is referred to the web version of this article.

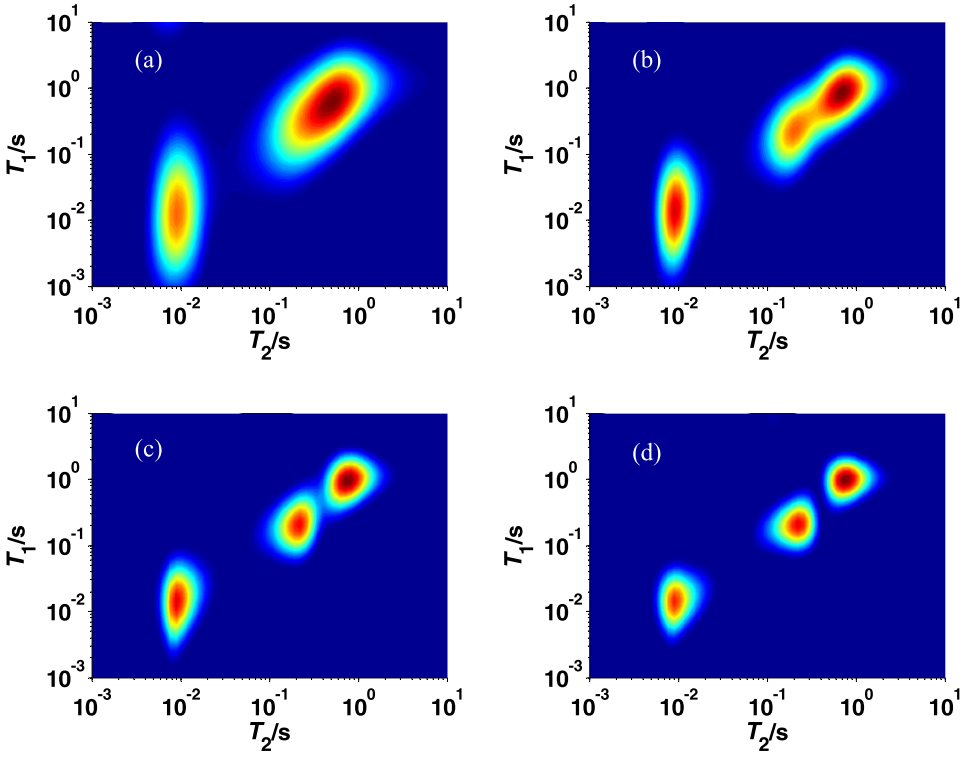

Fig. 8. Inverted T_1–T_2 maps of oil-water model with different SNRs using the curvature smoothing method. (a) SNR = 5; (b) SNR = 10; (c) SNR = 20; (d) SNR = 40.

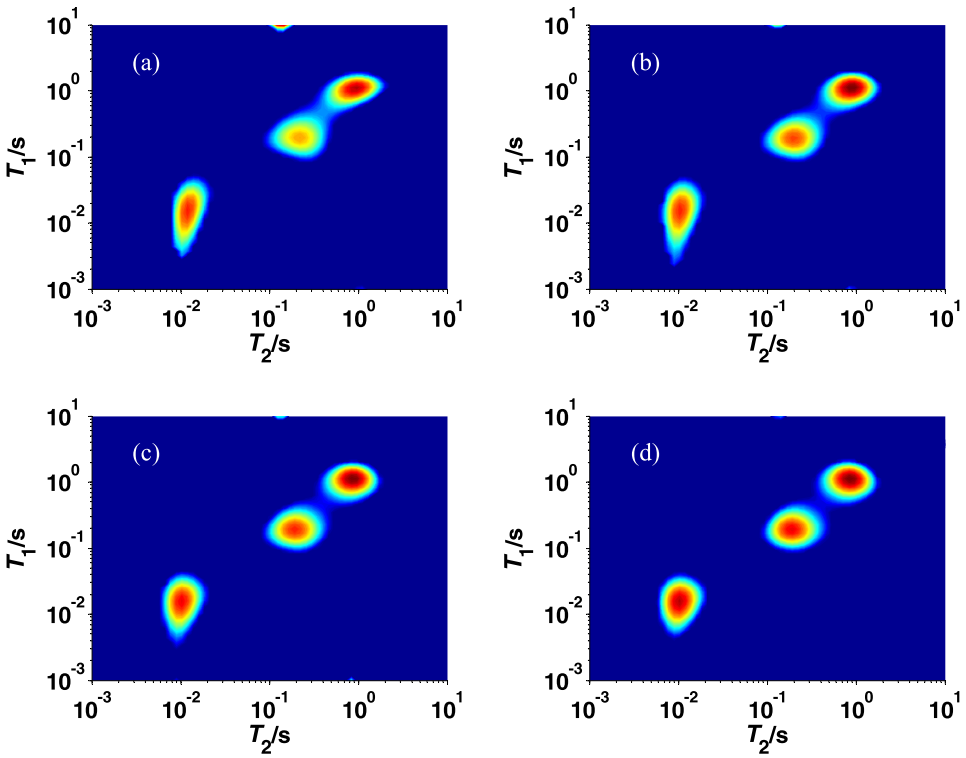

Fig. 9. Inverted T_1–T_2 maps of oil-water model with different SNRs using the proposed method. (a) SNR = 5; (b) SNR = 10; (c) SNR = 20; (d) SNR = 40.

4. Numerical examples

In this section, some numerical examples were implemented to validate the practicability and effectiveness of the proposed inversion method. Two formation T_1–T_2 map models with a porosity of 12 pu were developed, which are oil-water model and gas-water model. All the results were obtained from the same computer.

Table 1
Comparisons of the inversion results of different methods for oil-water model.

Method		SNR			
		40	20	10	5
TSVD	Porosity (pu)	12.73	13.34	13.41	13.50
	RE	0.79	0.82	0.85	0.85
Norm smoothing	Porosity (pu)	12.12	12.22	12.34	12.46
	RE	0.34	0.41	0.61	0.74
Curvature smoothing	Porosity (pu)	12.05	12.10	12.25	12.55
	RE	0.35	0.48	0.65	0.76
Proposed method	Porosity (pu)	12.04	12.10	12.15	12.18
	RE	0.28	0.33	0.40	0.55

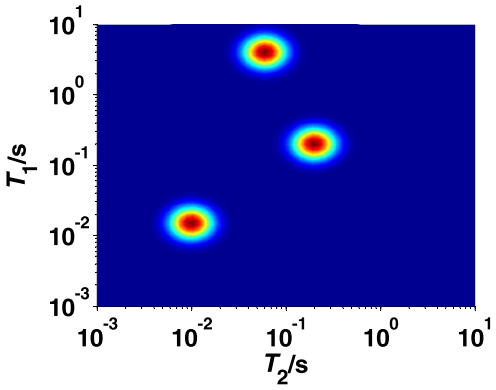

Fig. 10. Gas-water T_1–T_2 map model.

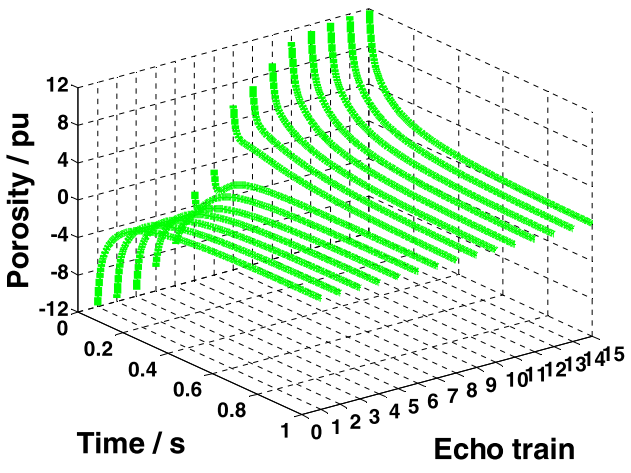

Fig. 11. Calculated echo data of gas-water model without noise.

4.1. Oil-water model

Oil-water T_1–T_2 map model containing bound water, free water and light oil was displayed in Fig. 4. The porosities of bound water, free water and light oil were all 4 pu, and their T_1 and T_2 were 0.01 s and 0.015 s, 0.2 s and 0.2 s, and 0.8 s and 1 s, respectively. The following forward parameters were set: the wait time group was [0.0001 0.0005 0.001 0.005 0.01 0.05 0.1 0.5 1.0 2.0 4.0 8.0 12.0 16.0 20.0] s; the echo spacing was 0.2 ms; the echo number was 10,000; and the components of T_1 and T_2 were each 64. The echo data with different wait times were calculated according to Eq. (2), as shown in Fig. 5, and Gaussian noises with different SNRs (5, 10, 20, and 40) were added to the calculated echo data and the corresponding noisy echo data were obtained. Subsequently, the echo number of the noisy data was compressed to 200 by the Gaussian-based random SVD method. Next, the compressed data were inverted by different inversion methods including the SVD method, norm smoothing method, curvature smoothing method, and the proposed method to obtain corresponding T_1–T_2 maps, as shown in Figs. 6–9.

It can be seen from Figs. 6–9 that the inverted T_1–T_2 maps using the TSVD method are very poor when the data SNR is lower than 40, which are exhibited that the light oil and water signals overlap each other exactly and bound water signal diverges obviously. The inverted T_1–T_2 maps using the norm smoothing method and the curvature smoothing method are similar when the data SNR is fixed, and when the data SNR reaches 40, the inverted T_1–T_2 maps are similar to the model, but the light oil and water signals overlap each other and bound water signal diverge obviously at SNR $\leq$ 20. Fortunately, the inverted T_1–T_2 maps using the proposed method can exhibit more focused fluid signals, which are exhibited that the light oil, free water, and bound water signals are separate when data SNR is low; this indicates that the proposed inversion method guarantees the sparsity of the solution and exhibits the strong robustness, and also suggests that the proposed method for choosing the optimum L1 regularization parameter and the proposed compression method and are acceptable. Therefore, the proposed inversion method is more competitive than the TSVD method, norm smoothing method, and the curvature smoothing method in aspects of NMR T_1–T_2 map inversion for oil-water model with a low SNR data.

Moreover, the porosity and the relative error of the inverted T_1–T_2 maps were calculated, as shown in Table 1. The porosity is calculated by summing the amplitude of T_1–T_2 map, and the relative error is determined from

$$\mathrm{RE} = \frac{\| \mathbf{S} - \mathbf{S}_{\mathrm{model}} \|_2}{\| \mathbf{S}_{\mathrm{model}} \|_2} \times 100\% \tag{22}$$

where RE is the relative error between the inverted T_1–T_2 map and the model; $\mathbf{S}$ is the inverted T_1–T_2 map; and $\mathbf{S}_{\mathrm{model}}$ is the T_1–T_2 map model.

From Table 1, it can be seen that the porosity of the inverted T_1–T_2 map from the proposed method is closest to the model porosity and the relative error is also lowest among the four inversion methods when the data SNR is fixed, which also verified the superiority of the proposed method to process T_1–T_2 data of oil-water model.

4.2. Gas-water model

Gas-water T_1–T_2 map model containing bound water, free water and gas was displayed in Fig. 10. The porosities of bound water, free water and gas were all 4 pu, and their T_1 and T_2 were 0.01 s and 0.015 s, 0.2 s and 0.2 s, and 4.0 s and 0.06 s, respectively. The following forward parameters were set: the wait time group was [0.0001 0.0005 0.001 0.005 0.01 0.05 0.1 1.0 2.0 4.0 8.0 12.0 16.0 24.0 40.0] s; the echo spacing was 0.2 ms; the echo number was 5000; and the components of T_1 and T_2 were each 64. The echo data

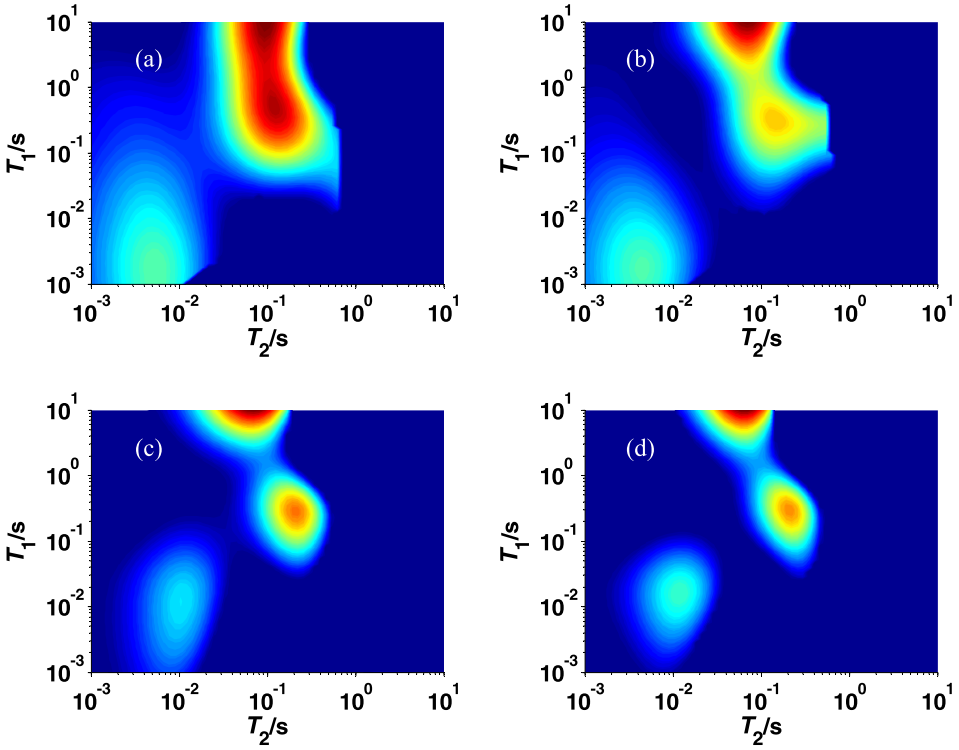

Fig. 12. Inverted T_1–T_2 maps of gas-water model with different SNRs using the TSVD method. (a) SNR = 5; (b) SNR = 10; (c) SNR = 20; (d) SNR = 40.

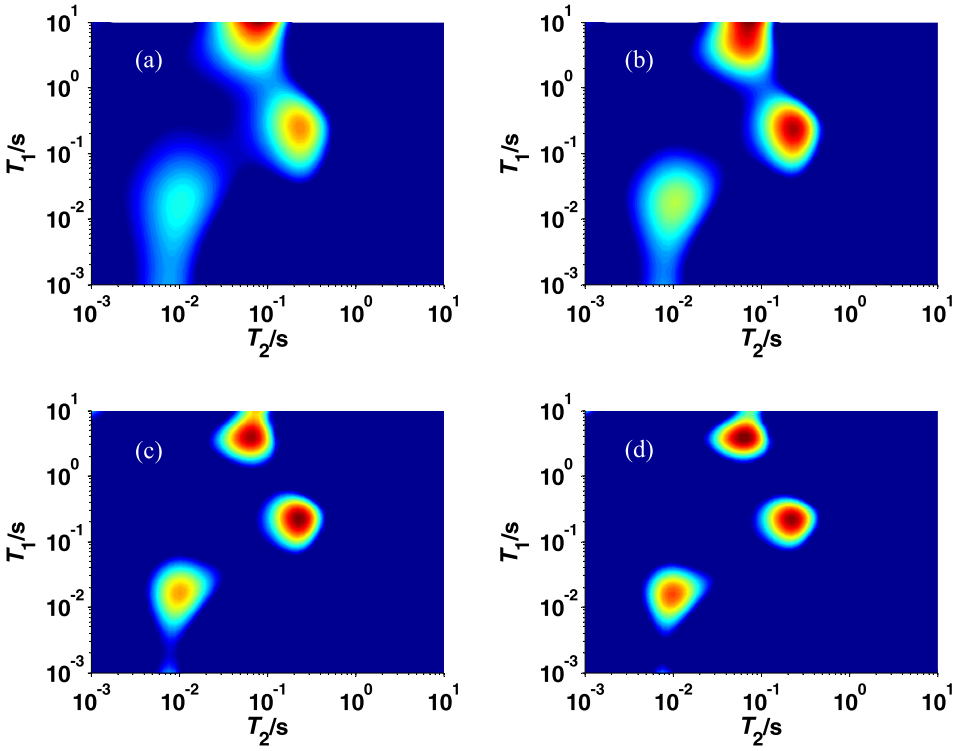

Fig. 13. Inverted T_1–T_2 maps of gas-water model with different SNRs using the norm smoothing method. (a) SNR = 5; (b) SNR = 10; (c) SNR = 20; (d) SNR = 40.

with different wait times were calculated according to Eq. (2), as shown in Fig. 11, and Gaussian noises with different SNRs (5, 10, 20, and 40) were added to the calculated echo data and the corresponding noisy echo data were obtained. Subsequently, the number of the noisy echo data was compressed to 200 using the Gaussian-based random SVD method. Next, the compressed data were inverted using different inversion methods including the SVD method, norm smoothing method, curvature smoothing method, and the proposed method to obtain corresponding T_1–T_2 maps, as shown in Figs. 12–15. Finally, the porosity and relative error of the inverted T_1–T_2 maps were calculated, as shown in Table 2.

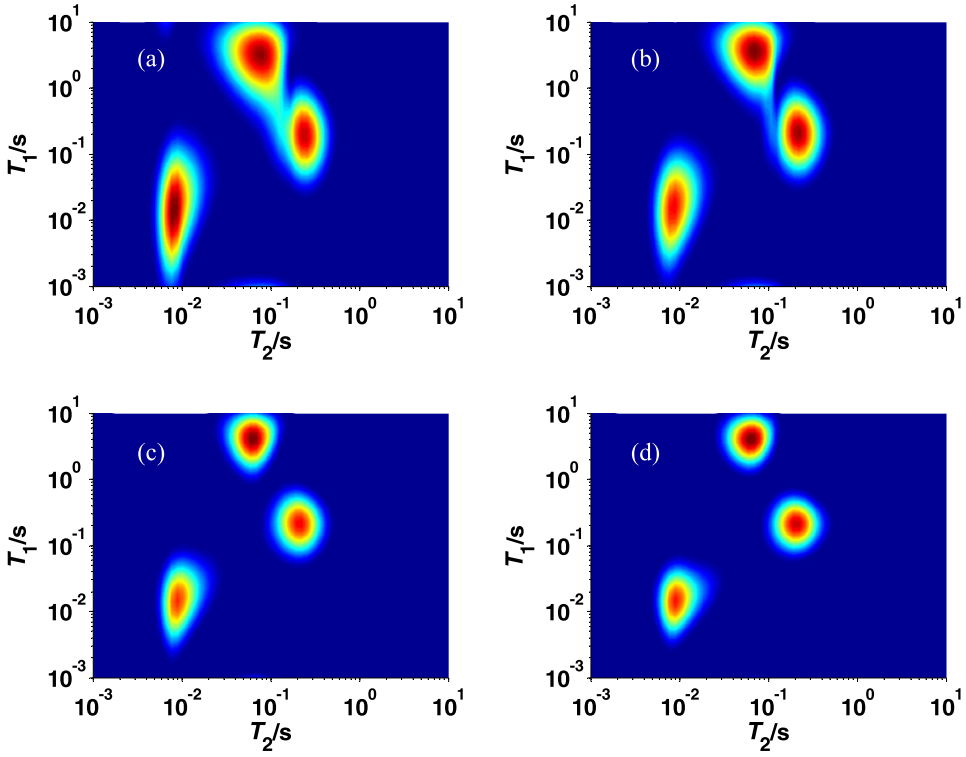

Fig. 14. Inverted T_1–T_2 maps of gas-water model with different SNRs using the curvature smoothing method. (a) SNR = 5; (b) SNR = 10; (c) SNR = 20; (d) SNR = 40.

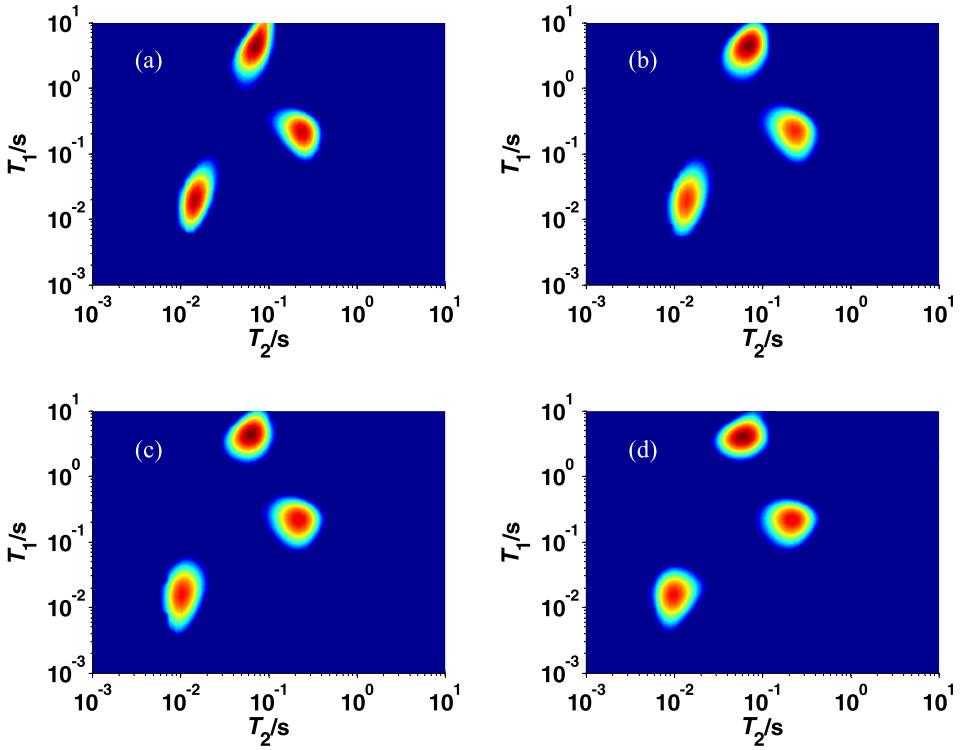

Fig. 15. Inverted T_1–T_2 maps of gas-water model with different SNRs using the proposed method. (a) SNR = 5; (b) SNR = 10; (c) SNR = 20; (d) SNR = 40.

From Figs. 12–15, it can be seen that the gas signal diverge obviously and is not displayed completely in the inverted T_1–T_2 map using the TSVD method, and the same is true for the inverted T_1–T_2 map using the norm smoothing method at SNR $\leq$ 10; the bound water, free water and gas signals in the inverted T_1–T_2 map using the proposed method are all focused well and do not overlap one another. Moreover, it can be seen from Table 2 that the inverted T_1–T_2 maps from the proposed method have a better porosity and a lower relative error with model over above mentioned inversion methods. Combined Figs. 12–15 and Table 2, a conclusion can be

Table 2
Comparisons of the inversion results of different methods for gas-water model.

Method		SNR			
		40	20	10	5
TSVD	Porosity (pu)	12.49	12.76	13.12	13.18
	RE	0.76	0.80	0.87	0.89
Norm smoothing	Porosity (pu)	12.10	12.19	12.35	12.46
	RE	0.36	0.46	0.64	0.76
Curvature smoothing	Porosity (pu)	12.07	12.11	12.19	12.31
	RE	0.38	0.47	0.67	0.77
Proposed method	Porosity (pu)	11.99	12.02	11.45	11.45
	RE	0.30	0.40	0.59	0.72

draw that the proposed inversion method exhibits the strong robustness for processing T_1–T_2 data of gas-water model.

After comprehensive analysis for oil-water model and gas-water model, it can be concluded that the proposed inversion method is robust and can achieve valuable solutions of NMR map inversion problem at a low data SNR.

5. NMR experiments

To validate the usefulness of the proposed inversion method to process actual NMR data, 2D T_1–T_2 experiments for $CuSO_4$ solutions with three concentrations and tight sandstone using IR-CPMG pulse sequence were implemented on a 2 MHz NMR Rock Core Analyzer produced by Magritek and the measured data were processed.

5.1. $CuSO_4$ solutions

The first $CuSO_4$ solution was formed by adding 0.005 g $CuSO_4{\cdot}5H_2O$ to 10 g water; the second one was formed by adding 0.03 g $CuSO_4{\cdot}5H_2O$ to 10 g water; and the third one was formed by adding 0.1 g $CuSO_4{\cdot}5H_2O$ to 10 g water. The three $CuSO_4$ solutions were measured separately through three groups of T_1–T_2 experiments, and then three $CuSO_4$ solutions were put together and measured by another experiment. During the experiments, the measured parameters were set as follow: the scanning number was 4; the echo spacing was 0.2 ms; the wait time group consisted of 20 values logarithmically spaced between 1 and 5000 ms; the echo number was 5000. Finally, the measured NMR data obtained from the four groups of T_1–T_2 experiments were processed using the proposed method and the corresponding T_1–T_2 maps were obtained, as shown in Fig. 16. The peak in Fig. 16(a) is located at (0.46, 0.46) s, the peak in Fig. 16(b) is located at (0.12, 0.12) s, and the peak in Fig. 16(c) is located at (0.02, 0.02) s. The three isolated peaks in Fig. 16(d) are located at (0.46, 0.46) s, (0.12, 0.12) s, and (0.02, 0.02) s from top-right to down-left. The location of each peak is correlated with the concentration of the $CuSO_4$ solution, and the higher concentration is, the longer relaxation time of the peak is. Moreover, the position of each peak in Fig. 16(d) corresponds to the peak position of independent solution. These phenomena are in good agreement with common sense, which revealing the effectiveness of the proposed method for processing NMR experimental data of the solutions.

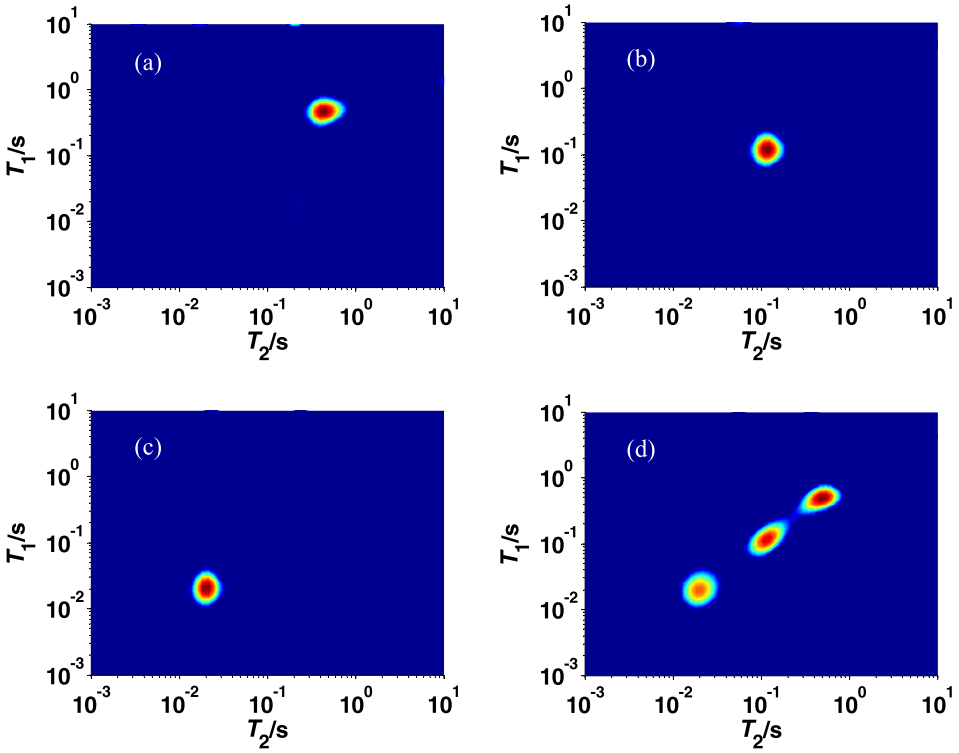

Fig. 16. Inverted T_1–T_2 maps of NMR experimental data for different $CuSO_4$ solutions using the proposed method. (a) The first $CuSO_4$ solution; (b) the second $CuSO_4$ solution; (c) the third $CuSO_4$ solution; (d) three $CuSO_4$ solutions together.

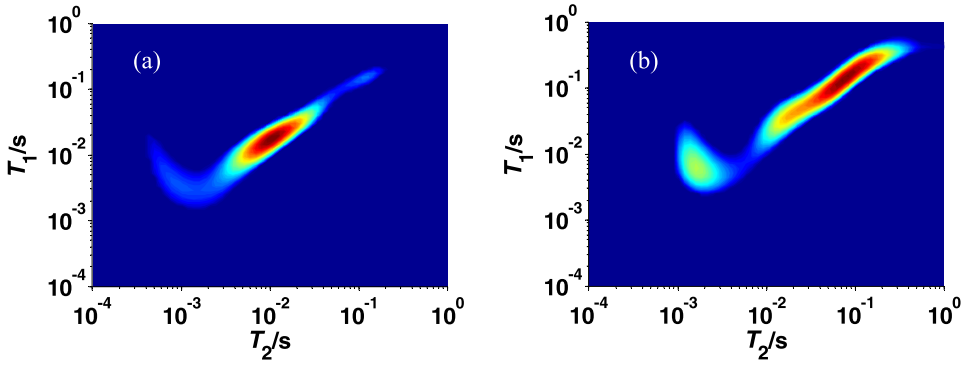

Fig. 17. Inverted T_1–T_2 maps of NMR experimental data for the water-saturated tight sandstone using the proposed method. (a) TS1 and (b) TS2.

5.2. Tight sandstone

Two cylindrical water-saturated tight sandstone cores were used in the NMR experiments. The first one named as "TS1" is characterized by a length of 4.51 cm, a diameter of 2.52 cm, and a gas porosity of 8.7 pu, and the second one named as "TS2" is characterized by a length of 5.17 cm, a diameter of 2.52 cm, and a gas porosity of 11.41 pu. During the experiments, the measured parameters were set as follow: the scanning number was 32; the echo spacing was 0.15 ms; the wait time group consisted of 20 values logarithmically spaced between 0.1 and 2000 ms; the echo number was 2000. Subsequently, the measured data were processed using the proposed method to obtain corresponding tight sandstone T_1–T_2 maps, as shown in Fig. 17. The calculated porosity of TS1 from the inverted T_1–T_2 map is 8.57 pu, and the calculated porosity of TS2 from the inverted T_1–T_2 map is 11.07 pu, which are very close to the gas porosity of the corresponding tight sandstone. Therefore, the proposed method can be used to process NMR experimental data of the rock.

After the analysis of the experiment results for the solutions and tight sandstones, it can be concluded that the proposed method is effective for processing NMR experimental data.

6. Conclusions and future works

In this study, a Gaussian-based random SVD method was proposed for compressing NMR data. Subsequently, a novel inversion method with double objective functions was proposed for T_1–T_2 data inversion. The first objective function was developed based on L1 regularization and solved by the TIST algorithm, and a new method for choosing the optimum L1 regularization parameter was proposed; the second objective function was developed based on the solution of the first objective function and solved by the CG algorithm. The effectiveness of proposed method was assessed through numerical and experimental investigations. The results suggested that the Gaussian-based random SVD method can implement T_1–T_2 data compression efficiently and reliably, the proposed method can choose the optimum L1 regularization parameter accurately and robustly, and the proposed inversion method works well and exhibits the strong robustness for NMR data inversion when data SNR is lower. Of course, the proposed methods can be extended to process other dimensional NMR data. For the future work, we will apply our proposed methods to processing NMR field data, while working on exploring more accurate inversion methods for a lower SNR data based on the idea of double objective functions.

Acknowledgements

The authors gratefully thank the financial supports from the National Natural Science Foundation of China (41674126).

References

[1] M.E. Smith, J.H. Strange, NMR techniques in materials physics: a review, Meas. Sci. Technol. 7 (1996) 449–475.
[2] D. Sebastiani, G. Goward, I. Schnell, M. Parrinello, NMR chemical shifts in periodic systems from first principles, Comput. Phys. Commun. 147 (2002) 707–710.
[3] K.H. Hausser, H.R. Kalbitzer, NMR in Medicine and Biology: Structure Determination, Tomography, in Vivo Spectroscopy, Springer Science & Business Media, 2012.
[4] G.R. Coates, L.Z. Xiao, M.G. Prammer, NMR Logging: Principles and Applications, Gulf Professional Publishing, Houston, Texas, USA, 1999.
[5] K.J. Dunn, D.J. Bergman, G.A. LaTorraca, Nuclear Magnetic Resonance Petrophysical and Logging Application, Elsevier Science Ltd., 2002.
[6] M.G. Prammer, NMR pore size distributions and permeability at the well site, Proc. SPE Annu. Techn. Conf. Exhib., 1994.
[7] N.J. Heaton, C.C. Minh, J. Kovats, U. Guru, Saturation and viscosity from multidimensional nuclear magnetic resonance logging, Proc. SPE Annu. Techn. Conf. Exhib., 2004.
[8] M. Liu, R. Xie, J. Guo, G. Jin, Characterization of pore structures of tight sandstone reservoirs by multifractal analysis of the NMR T2 distribution, Energy Fuel. 32 (2018) 12218–12230.
[9] G. Jin, R. Xie, M. Liu, J. Guo, Petrophysical parameter calculation based on NMR echo data in tight sandstone (in press) IEEE Trans. Geosci. Remote Sens. (2019), https://doi.org/10.1109/TGRS.2019.2901119.
[10] C. Liang, L. Xiao, C. Zhou, Y. Zhang, G. Liao, Z. Jia, Two-dimensional nuclear magnetic resonance method for wettability determination of tight sand, Magn. Reson. Imag. 56 (2019) 144–150.
[11] M.J. Tan, Y.L. Zou, J.Y. Zhang, Numerical simulation of (T2, T1) 2D NMR and fluid responses, Appl. Geophy. 19 (2012) 401–413.
[12] L. Venkataramanan, Y. Song, M.D. Hurlimann, Solving Fredholm integrals of the first kind with tensor product structure in 2 and 2.5 dimensions, IEEE Trans. Sign. Process. 50 (2002) 1017–1026.
[13] Y. Song, L. Venkataramanan, M. Hurlimann, M. Flaum, P. Frulla, C. Straley, T1–T2 correlation spectra obtained using a fast two-dimensional Laplace inversion, J. Magn. Reson. 154 (2002) 261–268.
[14] J. Butler, J. Reeds, S. Dawson, Estimating solutions of first kind integral equations with nonnegative constraints and optimal smoothing, SIAM J. Num. Anal. 18 (1981) 381–397.
[15] W.H. Press, S.A. Teukolsky, W.T. Vetterling, B.P. Flannery, Numerical Recipes 3rd edition: The Art of Scientific Computing, Cambridge University Press, 2007.
[16] S.W. Provencher, CONTIN: a general purpose constrained regularization program for inverting noisy linear algebraic and integral equations, Comput. Phys. Commun. 27 (1982) 229–242.
[17] É. Chouzenoux, S. Moussaoui, J. Idier, F. Mariette, Efficient maximum entropy reconstruction of nuclear magnetic resonance T1–T2 spectra, IEEE Trans. Sign. Process. 58 (2010) 6040–6051.
[18] Y. Zou, R. Xie, Y. Ding, A. Arad, Inversion of nuclear magnetic resonance echo data based on maximum entropy, Geophysics 81 (2016) D1–D8.
[19] X. Zhou, G. Su, L. Wang, S. Nie, X. Ge, The inversion of 2D NMR relaxometry data using L1 regularization, J. Magn. Reson. 275 (2017) 46–54.
[20] A. Reci, A.J. Sederman, L.F. Gladden, Obtaining sparse distributions in 2D inverse problems, J. Magn. Reson. 281 (2017) 188–198.
[21] J. Guo, R. Xie, M. Liu, A robust algorithm for 2D NMR diffusion-relaxation spectra inversion, IEEE Geosci. Remote Sens. Lett. 15 (2018) 1545–1549.
[22] P. Berman, O. Levi, Y. Parmet, M. Saunders, Z. Wiesman, Laplace inversion of low-resolution NMR relaxometry data using sparse representation methods, Concept. Magn. Reson. A 42 (2013) 72–88.
[23] P. Wang, L. Venkataramanan, V. Jain, Sparse clustered bayesian-inspired T1–T2 inversion from borehole NMR measurements, IEEE Trans. Comput. Imag. 3 (2017) 355–368.
[24] J. Guo, R. Xie, Y. Zou, G. Jin, L. Gao, C. Xu, A new method for NMR data inversion based on double-parameter regularization, Geophysics 83 (2018) JM39–JM49.

[25] X. Zhou, S. Nie, Y. Wang, Y. Zhang, Y. Yang, P. Yang, An iterative truncated singular value decomposition (TSVD)-based inversion methods for 2D NMR, Chin. J. Magn. Reson. 30 (2013) 541–551.
[26] X. Ge, H. Wang, Y. Fan, Y. Cao, H. Chen, R. Huang, Joint inversion of T1–T2 spectrum combining the iterative truncated singular value decomposition and the parallel particle swarm optimization algorithms, Comput. Phys. Commun. 198 (2016) 59–70.
[27] X. Hu, Y. Fan, H. Sun, L. Wang, Z. Wu, A novel efficient inversion method for three-dimensional NMR and the optimization of activation sequences and acquisition parameters, Comput. Geosci. 22 (2018) 867–883.
[28] R.C.O. Sebastião, J.P. Braga, Retrieval of transverse relaxation time distribution from spin-echo data by recurrent neural network, J. Magn. Reson. 177 (2005) 146–151.
[29] R.C.O. Sebastião, C.N. Pacheco, J.P. Braga, D. Piló-Veloso, Diffusion coefficient distribution from NMR-DOSY experiments using Hopfield neural network, J. Magn. Reson. 182 (2006) 22–28.
[30] C.C. Paige, M.A. Saunders, LSQR: sparse linear equations and least squares problems, ACM Trans. Math. Software 8 (1982) 195–209.
[31] M. Tan, Y. Zou, C. Zhou, A new inversion method for (T2, D) 2D NMR logging and fluid typing, Comput. Geosci. 51 (2013) 366–380.
[32] G. Su, X. Zhou, L. Wang, Y. Wang, S. Nie, An inversion method of 2D NMR relaxation spectra in low fields based on LSQR and L-curve, J. Magn. Reson. 265 (2016) 146–152.
[33] Z. Wang, L. Xiao, T. Liu, A new method for multi-exponential inversion of NMR relaxation measurements, Sci. China (Series G) 47 (2004) 265–276.
[34] Y. Zou, R. Xie, A novel method for NMR data compression, Comput. Geosci. 19 (2015) 389–401.
[35] J. Guo, R. Xie, G. Jin, An efficient method for NMR data compression based on fast singular value decomposition, IEEE Geosci. Remote Sens. Lett. 16 (2019) 301–305.
[36] N. Ailon, E. Liberty, Fast dimension reduction using Rademacher series on dual BCH codes, Discr. Comput. Geomet. 42 (2009) 615–630.
[37] J.M. Bioucas-Dias, M.A.T. Figueiredo, A new TwIST: two-step iterative shrinkage/thresholding algorithms for image restoration, IEEE Trans. Image Process. 16 (2007) 2992–3004.
[38] I. Daubechies, M. Defrise, C. De Mol, An iterative thresholding algorithm for linear inverse problems with a sparsity constraint, Commun. Pure Appl. Math. LVII (2004) 1413–1457.
[39] B. Chatterjee, Steepest Descent Method, Springer, Boston, USA, 2013.
[40] S.G. Nash, A survey of truncated-Newton methods, J. Comput. Appl. Math. 124 (2000) 45–59.
[41] P.S. Chang, A.N. Willson, Analysis of conjugate gradient algorithms for adaptive filtering, IEEE Trans. Sign. Proces. 48 (2000) 409–418.
[42] Y. Zou, R. Xie, A. Arad, Numerical estimation of choice of the regularization parameter for NMR T2 inversion, Petrol. Sci. 38 (2016) 237–246.